

Universal relation with regime transition for sediment transport in fine-grained rivers

Hongbo Ma^{a,1}, Jeffrey A. Nittrouer^{a,1}, Baosheng Wu^b, Michael P. Lamb^c, Yuanfeng Zhang^d, David Mohrig^e, Xudong Fu^{b,1}, Kensuke Naito^f, Yuanjian Wang^d, Andrew J. Moodie^a, Guangqian Wang^b, Chunhong Hu^g, and Gary Parker^{h,i,1}

^aDepartment of Earth, Environmental and Planetary Sciences, Rice University, Houston, TX 77251; ^bState Key Laboratory of Hydrosience and Engineering, Tsinghua University, 100084 Beijing, China; ^cDivision of Geological and Planetary Sciences, California Institute of Technology, Pasadena, CA 91125; ^dYellow River Institute of Hydraulic Research, 450000 Zhengzhou, China; ^eJackson School of Geosciences, The University of Texas at Austin, Austin, TX 78705; ^fCentro de Investigación y Tecnología del Agua, Universidad de Ingeniería y Tecnología, Barranco 15063, Peru; ^gState Key Laboratory of Simulation and Regulation of Water Cycle in River Basin, Institute of Water Resources and Hydropower Research, 100038 Beijing, China; ^hDepartment of Civil and Environmental Engineering, Ven Te Chow Hydrosystems Laboratory, University of Illinois at Urbana-Champaign, IL 61801; and ⁱDepartment of Geology, University of Illinois at Urbana-Champaign, IL 61801

Contributed by Gary Parker, October 31, 2019 (sent for review July 1, 2019; reviewed by Ton Hoitink and Heidi Nepf)

Fine-grained sediment (grain size under 2,000 μm) builds floodplains and deltas, and shapes the coastlines where much of humanity lives. However, a universal, physically based predictor of sediment flux for fine-grained rivers remains to be developed. Herein, a comprehensive sediment load database for fine-grained channels, ranging from small experimental flumes to megarivers, is used to find a predictive algorithm. Two distinct transport regimes emerge, separated by a discontinuous transition for median bed grain size within the very fine sand range (81 to 154 μm), whereby sediment flux decreases by up to 100-fold for coarser sand-bedded rivers compared to river with silt and very fine sand beds. Evidence suggests that the discontinuous change in sediment load originates from a transition of transport mode between mixed suspended bed load transport and suspension-dominated transport. Events that alter bed sediment size near the transition may significantly affect fluviocoastal morphology by drastically changing sediment flux, as shown by data from the Yellow River, China, which, over time, transitioned back and forth 3 times between states of high and low transport efficiency in response to anthropic activities.

sediment transport | fine-grained environments | regime transition | critical suspension number | universality

Evaluating fluvial sediment movement requires predictors of sediment transport rate. Among sedimentary environments on Earth, fine-grained lowland environments with median bed grain diameters of silt to sand ($D_{50} = 4$ to 2,000 μm) include rivers, floodplains, and deltaic, coastal, marine, subglacial, and volcanic systems (1–8). Low-lying fluviocoastal regions, threatened by reduced sediment supply and rising sea levels, provide living space for >40% of the world's population (9, 10). An algorithm for sand and silt transport is necessary to accurately forecast the transport of this material, and is also essential for evaluating fluviocoastal landscape evolution under changing environmental conditions.

Several physically based models have been developed for rivers with fine sand and coarser sand beds ($D_{50} > 150 \mu\text{m}$), herein referred to as typical sand bed rivers (11–14). These relations do not apply to silt and very fine sand bed rivers ($D_{50} < 150 \mu\text{m}$), herein referred to as silt-sand bed rivers (15–17). Despite making up a small proportion (~20%) of all lowland rivers (18), silt-sand bed rivers disproportionately contribute to sediment delivery to the coastline, and are some of the most morphologically active regions on Earth. The Yellow River, a typical silt-sand system ($D_{50} = 15$ to 150 μm), delivers 7% of world riverine sediment to the coastline using only 0.11% of riverine flow (19–21). The active lobe of the Yellow River delta extends ~1.5 km annually, representing the fastest-growing delta worldwide. In the Pilcomayo River (South America, $D_{50} \approx 100 \mu\text{m}$), the large sediment load blocks the channel and causes water to spill onto the floodplain,

instigating border disputes between Argentina and Paraguay (7). The Bermejo River, Argentina, is another example of a silt-sand river ($D_{50} \approx 80 \mu\text{m}$) where the lateral migration rate is 3 orders of magnitude higher than the adjacent Paraguay River that has a typical sand bed ($D_{50} \approx 180 \mu\text{m}$) (22, 23).

A universal sediment transport formulation for fine-grained rivers ($D_{50} < 2,000 \mu\text{m}$) should be applicable over a wide range of flow conditions, grain sizes, and environments, and should be well tested in both field and experimental settings. Yet, despite efforts over the past 70 y (11–14, 24, 25), even the best predictive algorithms show strong scale dependencies (12, 25), and fail for median grain sizes less than ~150 μm (15–17). For example, sediment load in the Yellow River is often 1 to 2 orders of magnitude greater than that predicted by Engelund–Hansen (EH) (17), the most widely validated relation for typical sand bed rivers (11, 12). Sediment transport relations have been developed for fine-grained rivers, like the Yellow River (16, 17), but these relations are not universal and have been calibrated for specific river reaches, laboratory data, or only certain scales (refs. 12, 16, 17, and 25; *SI Appendix, Text S1*).

Significance

Fine-grained sediment transport systems (grain size under 2,000 μm) are ubiquitous over time and space on Earth and extraplanetary surfaces, and include rivers, deltaic coastal settings, and submarine, lahar, and subglacial systems. Forecasting the evolution of Earth's surface requires a predictive algorithm for sediment transport. Herein we provide a universal relation for sediment transport in fine-grained rivers. Surprisingly, it is shown that sediment flux differs by up to 2 orders of magnitude as grain size changes only slightly near the boundary between very fine sand and fine sand. The universal applicability of the sediment transport formulation enables quantitative understanding of the sedimentology and morphology of fine-grained rivers.

Author contributions: H.M., J.A.N., and G.P. designed research; H.M., J.A.N., B.W., Y.Z., D.M., X.F., K.N., Y.W., A.J.M., G.W., and C.H. performed research; H.M. and X.F. contributed new reagents/analytic tools; H.M., M.P.L., and G.P. analyzed data; and H.M., J.A.N., M.P.L., and G.P. wrote the paper.

Reviewers: T.H., Wageningen University & Research; and H.N., Massachusetts Institute of Technology.

The authors declare no competing interest.

Published under the [PNAS license](https://www.pnas.org/licenses).

¹To whom correspondence may be addressed. Email: bigmatton@gmail.com, nittrouer@rice.edu, xdfu@tsinghua.edu.cn, or parkerg@illinois.edu.

This article contains supporting information online at <https://www.pnas.org/lookup/suppl/doi:10.1073/pnas.1911225116/-DCSupplemental>.

First published December 18, 2019.

Here we compile a sediment transport database for fine-grained bed rivers including 783 field and 811 laboratory studies (*SI Appendix, Table S1*) to derive a universal transport relation. The relation is an improvement over previous work because it avoids case dependence and can be applied across a range of flow conditions, environments, and scales; meanwhile, it provides insight into the linkages between notably high sediment concentrations in silt-sand bed rivers and lower values in typical sand bed rivers.

The Enigma of Exceptional Sediment Load in the Yellow River

We start by highlighting the apparent sediment transport anomaly of rivers with beds of silt and very fine sand, focusing on data from the lower Yellow River, China. These data (26) have been used to establish a generalized EH formulation (GEH), comparable to data from medium and coarse sand-bed channels (27), including those used to establish the EH relation (11). Fig. 1A illustrates a drastic discrepancy between the Yellow River and the data behind the sand-bed EH. Both datasets can be fitted to the form

$$C_f q_s^* = \alpha \tau^{*n}, \quad [1]$$

where $q_s^* = q_s / \sqrt{RgD^3} =$ Einstein number; $\tau^* = \tau / (R\rho gD) =$ Shields number; $C_f = gHS/U^2$ is the resistance coefficient (assuming steady, uniform flow); q_s is volumetric sediment flux per unit width (square meters per second); R is sediment submerged specific density; g is gravitational acceleration rate (meters per square second); D is median grain size or geometric mean grain size of bed material (meters); $\tau = \rho gHS = \rho C_f U^2 = \rho u_*^2$ is bed shear stress (pascals) for steady, uniform flow; ρ is water density (kilograms per cubic meter); H is water depth (meters); S is water surface slope; U is depth-averaged velocity (meters per second); and u_* is shear velocity (meters per second). Both the resistance coefficient C_f and the Shields number τ^* are macro-scale hydraulic factors that lump effects over grain and bedform scales (e.g., skin friction and form drag; *SI Appendix, Text S2*).

The values for coefficient α and exponent n are drastically different for the standard sand-bed EH relation, that is, $(\alpha, n) = (0.05, 5/2)$, as compared to GEH relation for the Yellow River, that is, $(\alpha, n) = (0.9, 5/3)$. For the same shear stress, sediment transport predicted by the GEH relation much more efficiently utilizes shear stress to produce higher sediment concentrations; on the contrary, sediment transport utilizes shear stress less efficiently in the EH relation (*SI Appendix, Text S2*). The difference between the 2 predictions for sediment load is 1 to 2 orders of magnitude. Insofar as EH is the gold standard for sand-bed rivers (11, 12), we ask hypothetically, Is there something special about the Yellow River that makes it different from all other rivers? Our answer is no, but with an unexpected twist.

The Yellow River Has Field and Laboratory Siblings

The first step toward answering whether the exceptional load of the Yellow River is an anomaly is to search for analogs. Although many field examples of silt-sand bed rivers exist (7, 8, 18, 23, 28), few sediment transport data have been collected from them. One case with the necessary data—Indian Canal (28)—behaves similarly to the Yellow River (*SI Appendix, Fig. S1*), in which the water depth varies from 0.67 m to 3.56 m and median grain size is between 20 μm and 82 μm , values close to those obtained from the Yellow River bed. Beyond the limited field data, we compiled data from 5 experimental studies (24, 25, 29–31) for silt-sand bed material ($D_{50} = 11$ to 153 μm). Results show that the experimental studies, like Indian Canal, follow the GEH relation, and thus act like the Yellow River (Fig. 1 and *Movie S1*). Thus the Yellow River is not special or unique: Sediment transport data from laboratory-scale flumes using silt-sand mixed material (rather than sand only) are well quantified by the GEH formulation (Fig. 1), indicating a strong element of universality.

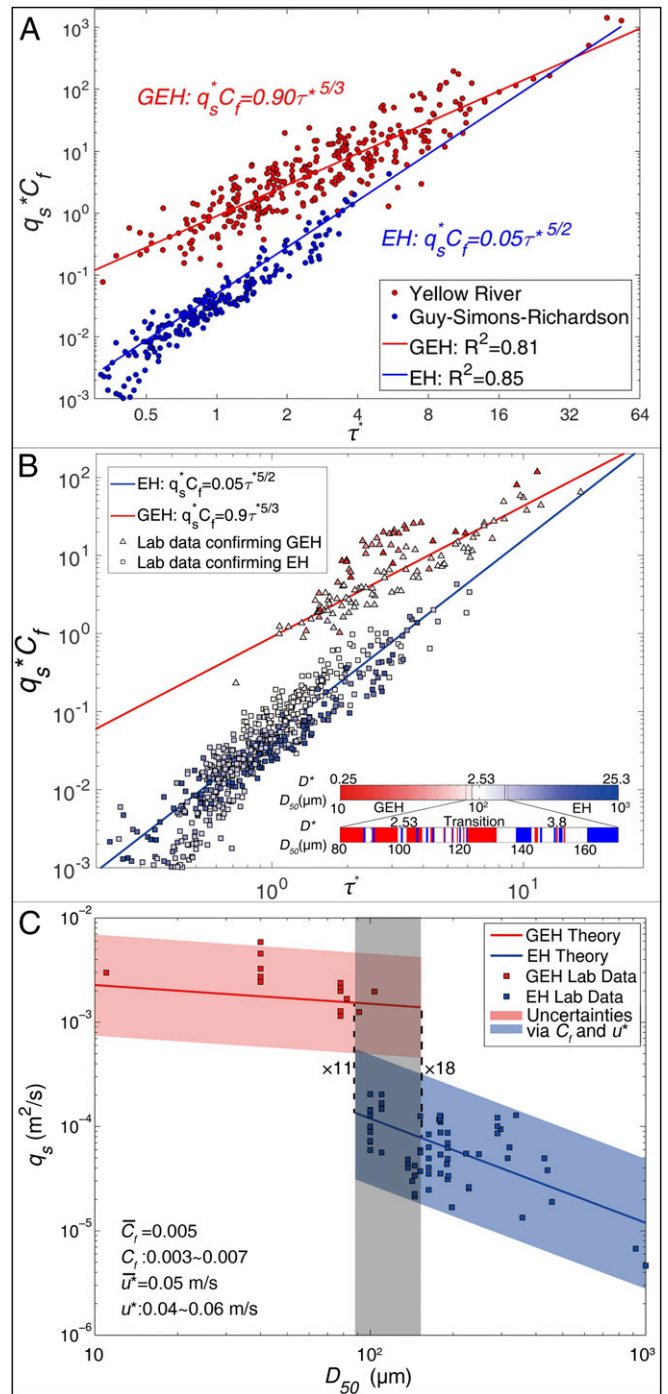


Fig. 1. Discontinuous regime transition behavior based on laboratory flume experiments. (A) GEH and EH formulations are compared to the databases (26, 27) that were used to develop them. (B) Comparison between sediment transport database and theoretical formulations in dimensionless space. Only laboratory data are shown here. Two distinct populations are evident, each of which is characterized by a similarity relation (power law), that is, GEH and EH. Data are colored to indicate the median grain size of the respective sediment bed; the corresponding color bar is shown inserted in the figure. Cases that agree with the GEH and EH formulations are shown in red and blue, respectively, on the lower bar. (C) Plot of dimensional sediment load (per unit width) and median grain size, which shows a discontinuous jump in sediment transport rate near $D_{50} = 100 \mu\text{m}$. Data within the range or parameter space (u^* , C_f) are shown in the plot. The mean values (overbars) of parameters are used to calculate the solid line for GEH and EH, and the uncertainty zones are calculated from the range of parameter space. This parameter space can be arbitrarily chosen to show the discontinuity, as also shown in *SI Appendix*. The difference between the 2 regimes is a factor of 11 to 18.

There is a clear discontinuity in sediment load between the typical sand bed datasets that plot along the EH relation and the silt-sand mixed channels that plot along the GEH relation (Fig. 1 and Movie S1). This discontinuity cannot be explained by the difference of experimental techniques, because there were 2 groups of data from the same setup (25), in which the silt bed experiment ($D_{50} = 40 \mu\text{m}$) agrees with GEH and the coarser experiment ($D_{50} = 110 \mu\text{m}$) agrees with EH. Moreover, this discontinuity may be separated to first order by a relatively narrow range of D_{50} : 88 to 153 μm (Fig. 1B). In dimensional space, for similar hydraulic conditions, sediment load q_s differs by a factor of 10 to 20 in the transitional zone of bed grain size (Fig. 1C). This discontinuous jump exists for every combination of hydraulic factors, and the discontinuity always occurs at the same grain size range (Fig. 1C and SI Appendix, Fig. S2). This behavior contradicts the assumption that a universal transport relation covering silt-sand and typical sand transport environments should be continuous (17, 25). We refer to this discontinuous relation between sediment load and grain size under similar hydraulic conditions as the *Fine-grained Transport Regime Transition* (FTRT), which separates the high transport efficiency regime for silt-sand beds that conform to GEH from the low transport efficiency regime for typical sand beds that follow EH.

Quantification of Regime Transition

The FTRT occurs over a narrow grain size range (Fig. 1), which suggests that grain size offers only first-order control, leaving at least one other parameter. Here we present and test 3 hypotheses, denoted H1 to H3, for the origin of the regime transition.

- 1) For H1, as bed material grain size declines, high-relief dunes of sand-bed rivers give way to low-relief bedforms generating little form drag, so that boundary shear stress is utilized maximally for sediment transport, prompting higher transport efficiency. Field evidence demonstrates that the high sediment load in a silt-sand system can coincide with a distinct change in bedform geometry (17). The transition between upper-regime plane bed and dune fields should also represent a discontinuous change related to hydraulic factors and grain size.
- 2) For H2, the FTRT arises where sediment transport makes a transition from a state of coexisting bed load and suspended load transport to predominantly suspension transport. This condition promotes low-relief bedforms, since the bed load necessary to construct large dunes is unavailable (32); hence, H1 and H2 are not mutually exclusive.
- 3) For H3, since the FTRT shows a remarkable dependence on grain size, a secondary parameter is hidden among factors associated with hydraulics or grain size distribution. Statistical information for grain size higher than first order, for example, the SD, may play an important role as a secondary parameter for demarcation of the 2 regimes of FTRT.

We test H1 with observations, since most of the flume experiments include documentation of bedforms. For this hypothesis to stand, it is necessary to show that high-relief bedforms lead to the EH regime, and low-relief bedforms lead to the GEH regime. However, while high-relief bedforms indeed lead to the EH regime, low-relief bedforms are a necessary but insufficient condition for GEH (Fig. 2A). Thus, H1 is not a complete explanation for the FTRT. Low-relief bedforms increase the effective shear stress for sediment transport; however, it may be that this condition is a consequence of augmented sediment transport rather than the cause.

The correspondence between bedform relief and transport regime, or lack thereof, sheds light on other possible hypotheses (H2 and H3). Several studies show that, when the ratio of suspended to total load is enhanced, high-relief bedforms give way to low-relief bedforms and a transition to upper-regime plane bed (32–34). However, upper-regime plane bed can also arise from bed load

sheet flow in the absence or near-absence of suspended load (35, 36). This is another line of evidence indicating that low-relief bedforms define a necessary but insufficient condition for high ratio of suspended to total load. The implication is that the GEH may be linked to a high ratio of suspended to total load, as predicated in H2.

To test H2, we seek cues from theoretical and experimental studies. Theoretically, in order to suspend a sediment particle directly from the bed surface, the suspension number ($Z_g = u^*/v_s$, where v_s is the settling velocity of the median bed material size) should be much greater than 2.5 (37). The widely adopted criterion, $Z_g > 3$, lacks justification (38). Nonetheless, a first test of this criterion shows that this value gives a lower bound for the transition to predominantly suspended load. $Z_g > 3$ is indeed necessary for the transition from EH to GEH, but the low-efficiency (EH, blue) and high-efficiency (GEH, red) points overlap in the range $3 \leq Z_g = u^*/v_s \leq 9.5$ (Fig. 2B). Notably, variation of Z_g is largely controlled by grain size (settling velocity); therefore, this level of overlap cannot be simply explained by the experimental uncertainties, because the grain size can be well constrained in the experiments. Thus, an additional parameter is necessary to separate the 2 regimes.

For H3, we use laboratory data to identify primary and secondary parameters that can separate the high- (GEH) and low-efficiency (EH) transport regimes. Upon evaluating 13 dimensionless numbers (SI Appendix, Table S2), we find that the suspension number Z_g (Fig. 2C) and the dimensionless grain size D^* ($D^* = (Rg/\nu^2)^{1/3}D$ (SI Appendix, Fig. S3), where ν is kinematic viscosity [square meters per second]) have first-order controls on the FTRT. However, these 2 numbers are somewhat equivalent in their capacities to separate the 2 regimes, because variation of $Z_g = u^*/v_s$ comes mostly from the settling velocity, which is, in turn, dictated by grain size; either may be used, but combining them does not improve predictive capability. We show results of both candidates later on. The only other term which contributes to a separation between the 2 regimes is the gradation coefficient, that is, $\sigma_D = (D_{84}/D_{16})^{0.5}$, which scales the SD of the bed grain size distribution. Thus, bed sorting plays a role in determining the FTRT. Specifically, Z_g or D^* offers first-order control on the FTRT, and σ_D (grain sorting or nonuniformity) offers second-order control (H3).

Using both laboratory and field data, we present the Z_g - σ_D regime diagram demarcating the transition (Fig. 2C). Note that the transitional value of Z_g ranges from a high of 9.5 for uniform sediment ($\sigma_D = 1$) to a low of 3.0 for $\sigma_D \geq 2$. Equivalently, we show a D^* - σ_D regime diagram demarcating the transition. The transitional value of D^* varies from 2.05 to 3.91 (D ranges from 81 μm to 154 μm for quartz in water on Earth) as σ_D varies from 1 to 2 (SI Appendix, Fig. S3). The principle used to develop the Z_g - σ_D and D^* - σ_D diagrams follows a criterion such that the diagram should minimize the number of statistical errors when predicting which transport regime each case belongs to.

The 2-parameter Z_g - σ_D regime transition criterion can be collapsed into a single criterion by using the entire grain size distribution. Let $f_{GSD}(D)$ denote the probability density function (PDF) of bed material grain size D . In many rivers with beds of sand and finer material, and, in particular, in the case of the lower Yellow River, this distribution can be approximated as log-normal (SI Appendix, Fig. S4), so that σ_D becomes synonymous with the geometric SD (39–42). For any given bed grain size distribution, the average value of the suspension number, here termed Z_{eff} , can be defined as $Z_{\text{eff}} = \int f_{GSD}(D)u^*/v_s(D)dD = u^*/v_{s-\text{eff}}$, where the effective fall velocity $v_{s-\text{eff}} = 1 / \int f_{GSD}(D)/v_s(D)dD$. Data analysis reveals a critical suspension number: $Z_{\text{eff},c} = 9.0 \pm 0.6$, such that the GEH regime prevails when $Z_{\text{eff}} > Z_{\text{eff},c}$ and the EH regime prevails when $Z_{\text{eff}} < Z_{\text{eff},c}$ (Fig. 2D and SI Appendix, Fig. S5). The fact that the FTRT is highly dependent on the critical suspension number supports H2, namely, that the FTRT corresponds to a transition between coexisting bed load and suspended load transport (EH) and predominantly suspension transport (GEH). The

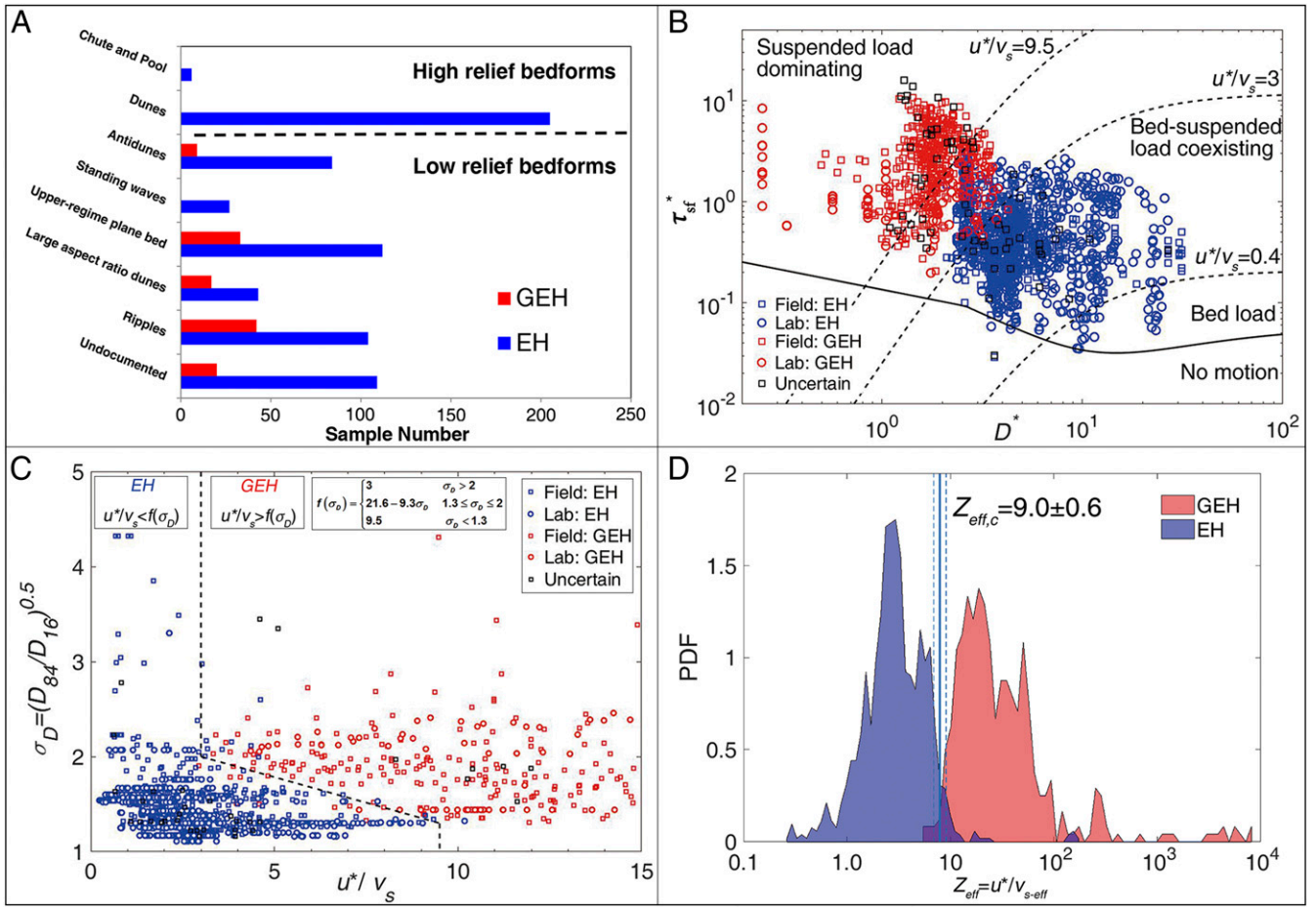


Fig. 2. Character of the FTRT. (A) Comparisons of bed states between GEH and EH (laboratory data only), whereby a necessary but insufficient condition to achieve the GEH regime is the presence of low-relief bedforms. (B) Transition between the transport modes, from coexistence of bed load and suspended load, to suspended load-dominated flows. Such transitions provide part of the physical basis for the FTRT mechanism. τ_{sf}^* is the dimensionless skin friction shear stress; D^* is the dimensionless median grain size. All of the data labeled “uncertain” were collected from field-scale canals or rivers (SI Appendix, Table S1). (C) Regime diagram of FTRT represented in terms of median suspension number $Z_g = u^*/v_s$ and geometric SD (gradation coefficient) σ_D of grain size. Both laboratory and field data are plotted, as well as an analytical expression for regime diagram demarcation. (D) Illustration of the emergence of a critical effective suspension number $Z_{eff,c} = 9.0 \pm 0.6$. Sediment transport is in GEH regime or in EH regime according to whether or not the effective suspension number $Z_{eff} = \int f_{GSD}(D) u^*/v_s(D) dD = u^*/v_{s-eff}$, respectively, greater or less than $Z_{eff,c}$ where $f_{GSD}(D)$ is the PDF of grain size. Solid line is the critical suspension number $Z_{eff,c} = 9.0$ and the dashed line is the uncertain range of $Z_{eff,c}$ (i.e., [8.4, 9.6]).

effect of gradation is such that poorly sorted sediment facilitates a transition from mixed bed and suspended load to a suspension-dominated mode at a higher median grain size D or a lower median suspension number Z_g within the transitional range ($D = 81$ to $154 \mu\text{m}$ or $Z_g = 3$ to 9.5). The critical suspension number can also explain why the 2 regimes cross at high stresses in Fig. 1. At such a high stress, Z_{eff} is likely to exceed $Z_{eff,c}$ and thus the 2 regimes would merge into the GEH regime (SI Appendix, Text S3 and Fig. S2A).

Universal Fine-Grained Sediment Transport Equation

We now join the EH and GEH formulations into a Universal EH relation (UEH) for fine-grained bed rivers (silt to sand bed). Based on Eq. 1 and Fig. 2D,

$$C_f q_s^* = \alpha \tau^{*n}, \quad [2A]$$

$$(\alpha, n) = \begin{cases} (\alpha, n)_{EH} = (0.05, 5/2) & \text{when } Z_{eff} < Z_{eff,c} \\ (\alpha, n)_{GEH} = (0.9, 5/3) & \text{when } Z_{eff} \geq Z_{eff,c} \end{cases}, \quad [2B]$$

where $Z_{eff} = \int f_{GSD}(D) u^*/v_s(D) dD = u^*/v_{s-eff}$, $Z_{eff,c} = 9.0$, $f_{GSD}(D)$ is the PDF of bed grain size and $v_{s-eff} = 1/\int f_{GSD}(D)/v_s(D) dD$. In alternative forms, Eq. 2B can be written by defining the transition

based on either Z_g or D^* (Fig. 2C and SI Appendix, Fig. S3). In the Z_g - σ_D diagram, $Z_g < f_{Z_g}(\sigma_D)$ for EH ($\alpha = 0.05$, $n = 5/2$) and $Z_g > f_{Z_g}(\sigma_D)$ for GEH ($\alpha = 0.9$, $n = 5/3$), where

$$f_{Z_g}(\sigma_D) = \begin{cases} 3 & \sigma_D > 2 \\ 21.06 - 9.3\sigma_D & 1.3 \leq \sigma_D \leq 2 \\ 9.5 & \sigma_D < 1.3 \end{cases}.$$

In the D^* - σ_D diagram, $D^* > f_D(\sigma_D) = 2.05 + 1.85/\{1 + \exp[-10(\sigma_D - 1.75)]\}$ for EH ($\alpha = 0.05$, $n = 5/2$) and $D^* < f_D(\sigma_D)$ for GEH ($\alpha = 0.9$, $n = 5/3$).

We test this formulation against our databases (Fig. 3), in which almost all of the data are independent of those used in the GEH and EH formulations. Results (Fig. 3 and SI Appendix, Table S3) show that the proposed universal sediment transport equation is roughly accurate to within a factor of 2 for any scale (geometric SD of discrepancy ratio less than 2), flow condition, and grain size, over 7 orders of magnitudes in Einstein number q_s^* . Such a strong agreement cannot be obtained using other formulations (SI Appendix, Text S1, Fig. S6, and Table S3), and no previous relations for fine-grained rivers (13, 17, 25) incorporate the FTRT.

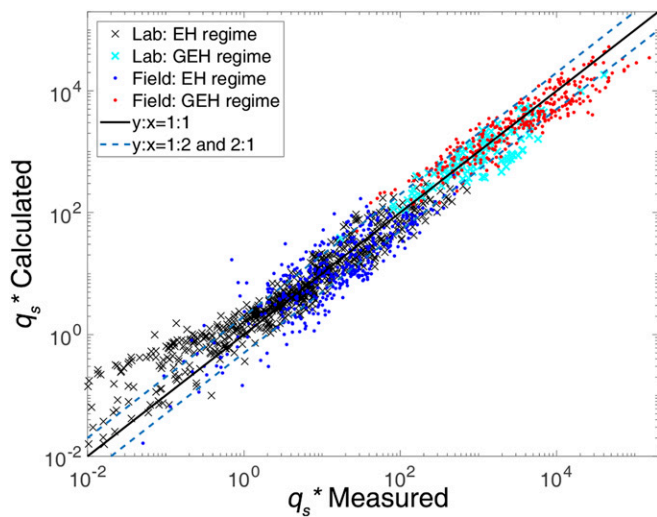


Fig. 3. Performance of UEH formulation against flume data and field data.

In Situ Measurements of Regime Transition

Rivers impacted by dams are likely locations to observe an FTRT, because the channel bed downstream tends to coarsen as fine sediment is winnowed out by clear water. We provide a case study from the lower Yellow River of China, where Sanmenxia Dam was constructed in 1960 and Xiaolangdi Dam was constructed in 1999 (*SI Appendix, Fig. S7*).

For Sanmenxia Dam, most of the upstream sediment was retained in the reservoir, so that water released was relatively clear. Over several years, the channel bed at Huayuankou (located ~ 275 km downstream) coarsened from $D_{50} \approx 70 \mu\text{m}$ to $D_{50} \approx 300 \mu\text{m}$. As sediment from the Loess Plateau (*SI Appendix, Fig. S7*) filled the reservoir rapidly, sediment bypassing was implemented in 1968. By the 1970s, the bed at Huayuankou recovered to its predam grain size composition ($D_{50} \approx 70 \mu\text{m}$) (43). Clear water releases are conducted yearly at Xiaolangdi Dam as part of the Water and Sediment Regulation operation, to degrade the bed and lower downstream flood stage. As a result, the bed at Huayuankou (~ 150 km downstream of Xiaolangdi Dam) again coarsened from $D_{50} \approx 70 \mu\text{m}$ to currently $D_{50} \approx 200 \mu\text{m}$ (ref. 44 and *SI Appendix, Table S4*). Our FTRT criteria predict that such changes in bed material size will result in alternation of the lower Yellow River between regimes of high (GEH) and low (EH) sediment transport efficiency.

Indeed, the FTRT is reflected in the order of magnitude variations in sediment transport rates measured at Huayuankou (Fig. 4): For 1961–1966 (bed D_{50} 194 to 400 μm) and 2001–2002 (bed D_{50} 200 to 210 μm), the data unambiguously fall in the EH regime (as predicted by UEH, i.e., Eq. 2). Comparatively, for 1980–1990 (bed D_{50} range 30 to 158 μm), the data fall in the GEH regime (as predicted by UEH). Therefore, our analyses indicate that there were 3 regime transitions induced by Sanmenxia and Xiaolangdi Dam operations: in the 1960s, GEH \rightarrow EH due to Sanmenxia Dam construction; in the 1970s, EH \rightarrow GEH due to the sediment bypass of Sanmenxia Dam and the recovery of the lower Yellow River to a silt-sand bed state; and lastly, in the late 1990s, GEH \rightarrow EH due to Xiaolangdi Dam construction. The sediment transport data collected at Huayuankou in 2001 and 2002 (i.e., 2 to 3 y after Xiaolangdi Dam; *SI Appendix, Table S4*) are in the EH regime, corresponding to rapid coarsening of the channel bed following dam construction.

Discussion

The FTRT corresponds to a critical suspension number $Z_{eff,c} = 9.0$, which satisfies the theoretical condition $Z_{eff,c} \gg 2.5$ for

direct suspension of bed particles (37). This finding indicates that the FTRT corresponds to a transition from mixed bed load and suspended load transport (EH) to suspension-dominated transport (GEH) (Fig. 2B). Experiments indicate that fine particles sheltered by large roughness structures can be directly entrained into a fluid without passing through a bed load layer, when the local viscous sublayer is penetrated by turbulent sweeps (45), indicating that the phenomena hypothesized to correspond with GEH indeed exists. The case where upper-regime plane bed is associated with the EH regime (low efficiency) can be explained by the presence of a substantial bed load layer, for example, an intense saltation layer or sheet flow. This would lower overall suspension in 2 ways: 1) extracting momentum and dissipating flow energy, thus lowering the mean shear stress at the fluid/bed load layer interface, and 2) diluting the sediment concentration at this interface relative to the underlying bed (35, 36). Alternatively, as the bed sediment becomes sufficiently fine, turbulent flow may become strong so that bed particles can be directly suspended into fluid without a bed load transitional layer (GEH).

There are limits to the UEH. First, the UEH, like other sediment transport formulae, is applicable for equilibrium transport of bed material load. Further developments are needed to describe nonequilibrium transport (46, 47). Second, the UEH relation has no critical shear stress and is not designed for the case of bed load only. This may explain the deviation between UEH and laboratory data, where very low sediment flux was observed (Fig. 3). Third, scatter may originate from inherent uncertainties associated with the flume and field data. The major uncertainties in the flume experiments include channel slope and bedform characterization. Moreover, difficulties in the measurement of bed material grain size, in both flume and field, may impede accurate discernment of bed material load. Fourth, the database compiled here comprises noncohesive sediment transport under turbulent flow conditions. Cohesive and hyperconcentrated sediment transport (48–50) is not considered. Sediment cohesion can reduce sediment entrainment (51, 52) and thus may reduce transport fluxes from those predicted by UEH.

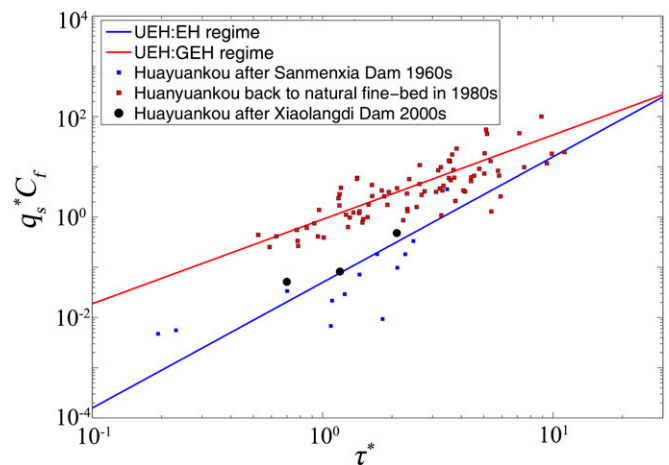


Fig. 4. Sediment transport regime transition measured in situ at Huayuankou, the Yellow River, China. The small blue squares correspond to the sediment transport regime in the 1960s, after the installation of Sanmenxia Dam caused coarsening of median bed grain size from $\sim 70 \mu\text{m}$ to $\sim 250 \mu\text{m}$. The points satisfy the EH relation. The small red squares correspond to conditions in the 1980s, after the reservoir behind the Sanmenxia Dam had filled with sediment and the bed median grain size had returned to $70 \mu\text{m}$. These red points satisfy the GEH relation. The black circles correspond to the sediment transport regime in the 2000s after the bed had coarsened again in response to construction of the Xiaolangdi Dam.

Conclusions

Sediment transport flux in fine-grained rivers does not vary smoothly as grain size increases. Instead, there exists a discontinuity in the range of very fine sand (81 to 154 μm) where sediment load decreases by 1 to 2 orders of magnitude (FTRT). The high-efficiency regime (GEH) has been observed in large rivers and canals, and is also present in experiments where the bed material is silt to fine sand. Theoretical and data analyses indicate that the FTRT corresponds to a transition in the sediment transport mode from suspension-dominated (GEH) to a mixed bed load and suspended load regime (EH). A dynamic transition between the high- and low-efficiency regimes, mediated by dam operation, has been observed 3 times within the Yellow River, China. Our UEH sediment transport relation,

validated for fine-grained rivers with grain sizes varying from 11 μm to 1080 μm , incorporates this FTRT.

ACKNOWLEDGMENTS. We thank the reviewers of this paper for their constructive comments. H.M., J.A.N., M.P.L., K.N., A.J.M., and G.P. gratefully acknowledge the NSF of the United States for support through Division of Earth Science (EAR) Grant 1427262. B.W. acknowledges support from the National Key R&D Program of China through Grant 2017YFC0405202. X.F. acknowledges support from the National Natural Science Foundation of China (NSFC) through Grants 51525901 and 91747207. Y.Z. acknowledges support from NSFC through Grant 51379087. Y.W. acknowledges support from NSFC through Grants 51539004, 51679104, and 51509102. A.J.M. acknowledges support from the NSF Graduate Research Fellowship under Grant 145068. H.M. acknowledges the financial support from the Department of Earth, Environmental and Planetary Sciences at Rice University. Data compiled for this study have been deposited on the online data archive figshare (DOI: 10.6084/m9.figshare.10060241).

1. G. S. Visher, Grain size distributions and depositional processes. *J. Sediment. Res.* **39**, 1074–1106 (1969).
2. J.-B. W. Stuut *et al.*, A 300-kyr record of aridity and wind strength in southwestern Africa: Inferences from grain-size distributions of sediments on Walvis Ridge, SE Atlantic. *Mar. Geol.* **180**, 221–233 (2002).
3. D. Sun *et al.*, Grain-size distribution function of polymodal sediments in hydraulic and aeolian environments, and numerical partitioning of the sedimentary components. *Sediment. Geol.* **152**, 263–277 (2002).
4. J. P. Grotzinger *et al.*; MSL Science Team, A habitable fluvio-lacustrine environment at Yellowknife Bay, Gale crater, Mars. *Science* **343**, 1242777 (2014).
5. L. M. Simkins *et al.*, Anatomy of a meltwater drainage system beneath the ancestral East Antarctic ice sheet. *Nat. Geosci.* **10**, 691–697 (2017).
6. J. Bohannon, Geophysics. Stalking a volcanic torrent. *Science* **316**, 1562–1563 (2007).
7. J. Martin-Vide, M. Amarilla, F. Zárate, Collapse of the Pilcomayo River. *Geomorphology* **205**, 155–163 (2014).
8. Q. Feng, Z. Li, G. Cheng, Grain size characteristics of sedimentary and the climatic change in middle reaches of Tarim River. *Chenji Xuebao* **14**, 227–233 (1996).
9. J. P. M. Syvitski, C. J. Vörösmarty, A. J. Kettner, P. Green, Impact of humans on the flux of terrestrial sediment to the global coastal ocean. *Science* **308**, 376–380 (2005).
10. J. E. Cohen, C. Small, A. Mellinger, J. Gallup, J. Sachs, Estimates of coastal populations. *Science* **278**, 1209–1213 (1997).
11. F. Engelund, E. Hansen, *A Monograph on Sediment Transport in Alluvial Streams* (Teknisk Forlag, Copenhagen, Denmark, 1967).
12. W. R. Brownlie, N. H. Brooks, *Prediction of Flow Depth and Sediment Discharge in Open Channels* (California Institute of Technology, Pasadena, CA, 1982).
13. L. C. van Rijn, Sediment transport, part II: Suspended load transport. *J. Hydraul. Eng.* **110**, 1613–1641 (1984).
14. H. Rouse, Modern conceptions of the mechanics of turbulence. *Trans. ASCE* **102**, 463–543 (1937).
15. Y. F. Zhang, Y. Q. Long, G. Q. Shen, “Adaptability of sediment transport formula to the Yellow River” in *Proceedings of the 7th International Symposium on River Sedimentation*, A. W. Jayawardena, J. H. W. Lee, Z. Y. Wang, Eds. (Taylor & Francis, 1998), pp. 87–92.
16. B. Wu, D. S. van Maren, L. Li, Predictability of sediment transport in the Yellow River using selected transport formulas. *Int. J. Sediment Res.* **23**, 283–298 (2008).
17. H. Ma *et al.*, The exceptional sediment load of fine-grained dispersal systems: Example of the Yellow River, China. *Sci. Adv.* **3**, e1603114 (2017).
18. G. V. Wilkerson, G. Parker, Physical basis for quasi-universal relationships describing bankfull hydraulic geometry of sand-bed rivers. *J. Hydraul. Eng.* **137**, 739–753 (2010).
19. P. Gleick, The world’s water. *Issues Sci. Technol.* **14**, 80–82 (1998).
20. J. D. Milliman, R. H. Meade, World-wide delivery of river sediment to the oceans. *J. Geol.* **91**, 1–21 (1983).
21. G. Orton, H. Reading, Variability of deltaic processes in terms of sediment supply, with particular emphasis on grain size. *Sedimentology* **40**, 475–512 (1993).
22. E. C. Drago, M. L. J. W. I. Amsler, Bed sediment characteristics in the Paraná and Paraguay Rivers. *Water Int.* **23**, 174–183 (1998).
23. G. H. Sambrook Smith, J. L. Best, J. Z. Leroy, O. Orfeo, The alluvial architecture of a suspended sediment dominated meandering river: The Rio Bermejo, Argentina. *Sedimentology* **63**, 1187–1208 (2015).
24. A. A. Kalinske, C. H. Hsia, *Study of Transportation of Fine Sediments by Flowing Water* (University of Iowa Studies in Engineering Bulletin, University of Iowa, Iowa City, IA, 1945), vol. 29.
25. E. M. Laursen, The total sediment load of streams. *J. Hydraul. Div.* **84**, 1–36 (1958).
26. Y. Q. Long, Y. F. Zhang, Study on the Yellow River sediment from the viewpoint of total sediment [in Chinese]. *Yellow River* **24**, 28–29 (2002).
27. H. P. Guy, D. B. Simons, E. V. Richardson, “Summary of alluvial channel data from flume experiments, 1956–61” (Rep. 2330-7102, United States Government Printing Office, Washington, DC, 1966).
28. S. V. Chitales, *Hydraulics of Stable Channels Tables 13 and 17* (Government of India, Ministry of Irrigation and Power, Central Water and Power Commission, 1966).
29. S. Wang, R. Zhang, “Experimental study on transport rate of graded sediment” in *Proceedings of International Conference on River Flood Hydraulics*, W. R. White, Ed. (John Wiley, 1990), pp. 299–306.
30. S. Wang, J. Cheng, Y. Hui, A study on the transport capacity of nonuniform sediment in open channels [in Chinese]. *J. Hydraul. Eng. Chin. Hydraul. Eng. Soc.* **1**, 1–9 (1998).
31. G. Kalkanis, “Observations of turbulent flow near an oscillating wall” (Tech. Memo 97, Beach Erosion Board, Washington, DC, 1957).
32. V. Ganti, M. P. Lamb, B. McElroy, Quantitative bounds on morphodynamics and implications for reading the sedimentary record. *Nat. Commun.* **5**, 3298 (2014).
33. D. Mohrig, J. D. Smith, Predicting the migration rates of subaqueous dunes. *Water Resour. Res.* **32**, 3207–3217 (1996).
34. S. Naqshband, A. J. F. Hoitink, B. McElroy, D. Hurther, S. J. M. H. Hulscher, A sharp view on river dune transition to upper stage plane bed. *Geophys. Res. Lett.* **44**, 11437–11444 (2017).
35. P. Gao, Transition between two bed-load transport regimes: Saltation and sheet flow. *J. Hydraul. Eng.* **134**, 340–349 (2008).
36. H. Capart, L. Fraccarollo, Transport layer structure in intense bed-load. *Geophys. Res. Lett.* **38**, L20402 (2011).
37. Y. Niño, M. García, Engelund’s analysis of turbulent energy and suspended load. *J. Eng. Mech.* **124**, 480–483 (1998).
38. M. P. Lamb, J. G. Venditti, The grain size gap and abrupt gravel-sand transitions in rivers due to suspension fallout. *Geophys. Res. Lett.* **43**, 3777–3785 (2016).
39. M. H. García, *Sedimentation Engineering: Processes, Measurements, Modeling, and Practice* (American Society of Civil Engineers, 2008).
40. A. Molinas, B. S. Wu, Effect of size gradation on transport of sediment mixtures. *J. Hydraul. Eng.* **124**, 786–793 (1998).
41. B. Wu, A. Molinas, P. Y. Julien, Bed-material load computations for nonuniform sediments. *J. Hydraul. Eng.* **130**, 1002–1012 (2004).
42. R. M. Dorrell, L. A. Amy, J. Peakall, W. D. McCaffrey, Particle size distribution controls the threshold between net sediment erosion and deposition in suspended load dominated flows. *Geophys. Res. Lett.* **45**, 1443–1452 (2018).
43. G. Q. Wang, B. S. Wu, Z. Y. Wang, Sedimentation problems and management strategies of Sanmenxia Reservoir, Yellow River, China. *Water Resour. Res.* **41**, W09417 (2005).
44. H. Wang *et al.*, Impacts of the dam-orientated water-sediment regulation scheme on the lower reaches and delta of the Yellow River (Huanghe): A review. *Global Planet. Change* **157**, 93–113 (2017).
45. Y. Niño, F. Lopez, M. García, Threshold for particle entrainment into suspension. *Sedimentology* **50**, 247–263 (2003).
46. M. García, G. Parker, Entrainment of bed sediment into suspension. *J. Hydraul. Eng.* **117**, 414–435 (1991).
47. S. Wright, G. Parker, Flow resistance and suspended load in sand-bed rivers: Simplified stratification model. *J. Hydraul. Eng.* **130**, 796–805 (2004).
48. T. C. Pierson, “Hyperconcentrated flow—Transitional process between water flow and debris flow” in *Debris-Flow Hazards and Related Phenomena*, M. Jakob, O. Hungr, Eds. (Springer, 2005), pp. 159–202.
49. J. Xu, Erosion caused by hyperconcentrated flow on the Loess Plateau of China. *Catena* **36**, 1–19 (1999).
50. J. Winterwerp, Stratification effects by cohesive and noncohesive sediment. *J. Geophys. Res. Oceans* **106**, 22559–22574 (2001).
51. M. G. Sassi, A. J. F. Hoitink, B. Vermeulen, Quantified turbulent diffusion of suspended sediment using acoustic Doppler current profilers. *Geophys. Res. Lett.* **40**, 5692–5697 (2013).
52. C. P. Van *et al.*, Modelling fine-grained sediment transport in the Mahakam land-sea continuum, Indonesia. *J. Hydro Environ. Res.* **13**, 103–120 (2016).